RAA 2017 Vol. **17** No. **6**, 60 (6pp) doi: 10.1088/1674–4527/17/6/60

http://www.raa-journal.org *http://iopscience.iop.org/raa*

Research in Astronomy and Astrophysics

Design and experimental test of an optical vortex coronagraph

Cheng-Chao Liu[1,2], De-Qing Ren[3,1,2], Yong-Tian Zhu[1,2] and Jiang-Pei Dou[1,2]

[1] National Astronomical Observatories/Nanjing Institute of Astronomical Optics & Technology, Chinese Academy of Sciences, Nanjing 210042, China; *ccliu@niaot.ac.cn*

[2] Key Laboratory of Astronomical Optics & Technology, National Astronomical Observatories/Nanjing Institute of Astronomical Optics & Technology, Chinese Academy of Sciences, Nanjing 210042, China

[3] Physics & Astronomy Department, California State University, Northridge, 18111 Nordhoff Street, Northridge, California 91330-8268, USA

Received 2017 January 5; accepted 2017 March 19

Abstract Using an optical vortex coronagraph (OVC) is one of the most promising techniques for directly imaging exoplanets because of its small inner working angle and high throughput. This paper presents the design and laboratory demonstration performance of an OVC based on liquid crystal polymers (LCPs) at 633 nm and 1520 nm. The OVC can deliver good performance in laboratory tests and achieve a contrast of 10^{-6} at an angular distance of 3λ/D, which can be implemented for imaging young giant exoplanets in combination with extreme adaptive optics.

Key words: instrumentation: coronagraph — techniques: optical vortex — methods: laboratory

1 INTRODUCTION

Nowadays, more than 3000 exoplanets have been discovered. Yet, most of these exoplanets have been identified by indirect detection techniques, such as radial velocity or transiting with very few exoplanets having been imaged. However, the direct imaging method acts as an important step in analyzing the atmospheric compositions of planets via spectroscopy since it can capture photons from planets. Due to the large difference in brightness between a host star and its planets as well as their small angular separation, direct imaging is extremely technologically challenging. High contrast imaging is a rapidly developing field. In space, a coronagraph can separate targets with a contrast ratio (hereafter simply called contrast) of $10^{-9} \sim 10^{-10}$ with different wavefront correction techniques, which can be used for the direct imaging of Earth-like planets (Trauger & Traub 2007; Dou & Ren 2016; Liu et al. 2015; Liu et al. 2016). On the ground, a coronagraph combined with extreme adaptive optics (ExAO) and associated image reduction techniques can reach contrasts of $10^{-6} \sim 10^{-7}$, which can be used for imaging young giant exoplanets (Vigan et al. 2016; Macintosh et al. 2014; Dou et al. 2015a). Recently, various concepts for coronagraphs have been proposed to suppress the central starlight; for example, amplitude apodization coronagraph (Kasdin et al. 2003; Guyon 2003), apodization pupil coronagraph (Ren & Zhu 2007; Dou et al. 2010; Soummer et al. 2003; Kuchner & Traub 2002) and phase mask coronagraph (Rouan et al. 2000; Abe et al. 2001; Foo et al. 2005; Mawet et al. 2005). Among these, a vortex coronagraph is a promising technique, which has many advantages including small inner working angle (IWA), which is one way to utilize in conjunction with a smaller telescope, high throughput (theoretically 100%), a clear 360° discovery region, low chromatic dependence and ease of installation in coronagraphic systems (Guyon et al. 2006).

Optical vortex coronagraphs (OVCs) can be divided into two types: scalar and vector. With technical advancements, a promising new technique based on birefringent liquid crystal polymers (LCPs) has been used to manufacture a vector optical vortex phase plate (Mawet et al. 2009). Nowadays, a dual-stage vortex coronagraph optimized for an on-axis telescope has been developed by the Jet Propulsion Laboratory (JPL) with a contrast of 10^{-5} at $2\lambda/D$ in the laboratory. This instrument was installed on the Hale Telescope at Palomar Observatory and can achieve a contrast of 10^{-4} at $2\lambda/D$ (Serabyn et al. 2016; Bottom et al. 2016). The Annular Groove Phase Mask

(AGPM) coronagraph developed by JPL can generate a contrast of 6×10^{-5} at $2\lambda/D$, and was installed on the Keck II Telescope (Delacroix et al. 2013; Serabyn et al. 2017). The vortex coronagraph was tested in JPL's High Contrast Imaging Testbed (HCIT) and a contrast below 10^{-9} has been demonstrated across "dark hole" regions (Serabyn et al. 2014).

Our coronagraph is based on a commercial half waveplate (HWP), which has few requirements for delivering good performance, thus saving labor and investment. By fully taking advantage of the high quality of commercial products, excellent performance can be achieved. It can yield a contrast of 10^{-6} at angular distance of $3\lambda/D$, which is one of the best performances available by using the vortex coronagraphic technique. This coronagraph will be installed on China's Lijiang 2.4-m telescope with our dedicated adaptive optics and polarimetry for direct imaging of exoplanets. It will be further developed for a future proposed Chinese 12-m Large Optical/Infrared Telescope.

We present the principle and instrument design in Section 2. A numerical simulation is shown in Section 3, and Section 4 describes the performance of the OVC. We conclude our results and outline future work in Section 5.

2 THE PRINCIPLE AND DESIGN OF OPTICAL VORTEX CORONAGRAPH

An OVC uses a helical phase following the form $e^{i\phi}$, with $\phi = l\theta$, where l is the topological charge and θ is the azimuthal coordinate of the focal plane. In optical systems, vortices manifest themselves as a dark donut of destructive interference that occurs at phase singularities (Rozas et al. 1997; Niv et al. 2006). We can use this dark core to attenuate an on-axis star so nearby planets can be imaged. An optical vortex beam propagating in the z direction can be expressed by the electric field (Vasnetsov & Staliunas 1999)

$$E(\rho, \phi, z, t) = A(\rho, z) \exp(il\theta) \exp(iwt - ikz), \quad (1)$$

where (ρ, ϕ, z) are cylindrical coordinates, $A(\rho, z)$ is a circularly symmetric amplitude function and $k = 2\pi/\lambda$ is the wavenumber of a monochromatic field with wavelength λ.

Figure 1 shows how to suppress the on-axis light using the vortex phase mask. The spiral phase plate is placed in the (x, y) plane and the center coincides with the origin of the coordinate system.

Different from other phase mask coronagraphs such as the four-quadrant phase mask, a rotationally symmetric HWP, manufactured using an LCP, which can generate an azimuthal phase spiral reaching an even multiple

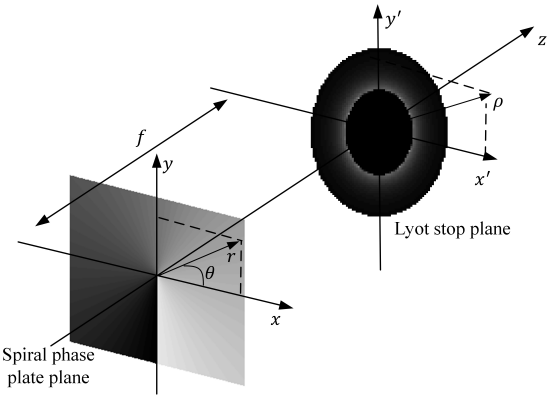

Fig. 1 Illustration of diffraction of vortex phase mask on the on-axis light. Most of the light will emerge outside of the geometrical circle, which can be blocked by a Lyot stop.

Fig. 2 The phase map of the LCP with $l = 2$ (*left*) and the photo of the LCP optimized at 633 nm (*right*).

of 2π radian in the circuit about the center, is used in our test (McEldowney et al. 2008a; McEldowney et al. 2008b). Thorlabs' LCP is a half wave retarder designed to affect the radial and azimuthal polarization of optical fields. An LCP offers constant retardance across the clear aperture but its fast axis rotates continuously over the area utilized by the optics about the center. An LCP with $l = 2$ is applied in our test and Figure 2 shows the phase changing from 0 to 4π radian and the photograph of the LCP HWP.

A preliminary schematic diagram of the OVC is shown in Figure 3. The coronagraph includes three Fourier transforming lenses L2, L3 and L4. The entrance plane wave of the starlight can be described by

$$U(x, y) = A(x, y). \quad (2)$$

Therefore, the electric field in the first focal plane is

$$U(u, v) = \exp(il\theta) FT(A(x, y)). \quad (3)$$

L3 performs an inverse Fourier transform on $U(x, y)$ and the electric field in the pupil plane can be expressed by

$$U(x', y') = P_{\mathrm{Lyot}}(x', y') FT^{-}(\exp(il\theta) FT(A(x, y))). \quad (4)$$

P_{Lyot} is the transmission function of the Lyot stop expressed by $P_{\mathrm{Lyot}}(x', y') = 1$ for $\rho = \sqrt{(x'^2 + y'^2)} <$

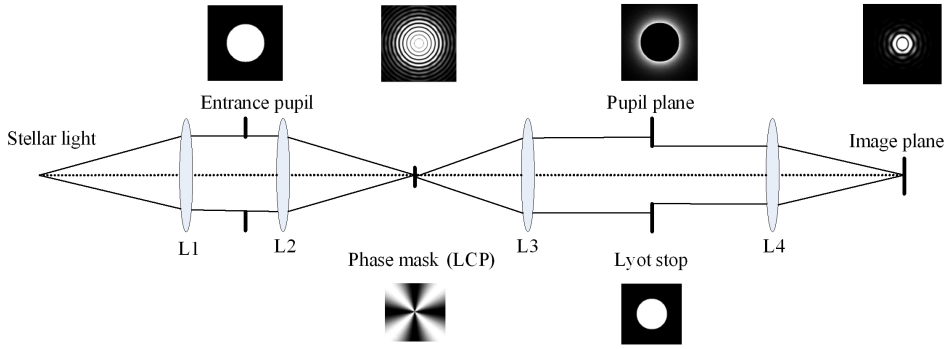

Fig. 3 Schematic of optical vortex coronagraph. The stellar light simulated by laser was firstly collimated by lens L1, then focused by lens L2 onto the phase mask (LCP). L3 reimages the entrance pupil where the diffracted light from the phase mask is blocked by the Lyot stop. L4 focuses the light on our camera.

$R_{\rm Lyot}$ and zero otherwise. The electric field on the final image plane can be described as

$$U(u', v') = FT[U(x', y')]. \quad (5)$$

The general model of the coronagraph presented in Figure 3 can be efficiently translated into a numerical code.

3 OPTICAL VORTEX CORONAGRAPH SIMULATION

We simulated the performance of the OVC according to the above equations. In order to obtain fine sampling of the coronagraphic images, we applied the Fourier Transform algorithm with 4096×4096 pixels in the simulation. In our simulations, we consider an ideal plane wavefront entering an unobstructed telescope with a circular aperture and diameter $D = 200$ pixels. The Lyot stop diameter $D_{\rm LS}$ is set to 0.8 times that of the entrance pupil. The topological charge of LCP is $l = 2$.

Figure 4 displays the simulated contrast achieved by the OVC with $l = 2$. From the figure we can conclude that the theoretical contrast of a vortex phase mask ($l = 2$) based on the numerical simulation can reach 10^{-7} at $2\lambda/D$ (blue line) compared to non-coronagraphic contrast (red line). Due to the sensitivity of the vortex coronagraph to the finite pixel sampling, which constrains the final result of the simulation, it cannot achieve the theoretical 100% nulling. Therefore, the contrast 10^{-7} represents a reasonable value for theoretical contrast with a reasonable number of pixels used for sampling.

We investigated contrast sensitivity of topological charge 2 on the central obstruction, low-order aberration and bandwidth. Like most coronagraphs, the contrast of OVC is also degraded by the central obstruction and spider.

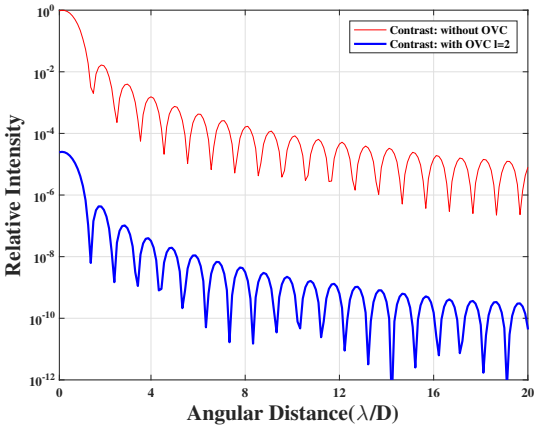

Fig. 4 The theoretical contrast with and without OVC.

Figure 5 shows the intensity distribution on Lyot stop plane (top) and the contrast sensitivity to the central obstruction at the angular separation $1\lambda/D$ (bottom). The problem of secondary obstruction can be solved by inducing a secondary vortex series (Mawet et al. 2011). The influence of low-order aberration on the contrast is displayed in Figure 6. Figure 7 demonstrates chromatic effects on the vortex coronagraph. One technique to solve the achromaticity of the vortex coronagraph is to use a stack of LCP layers (Mawet et al. 2010).

4 THE EXPERIMENTAL TEST OF OVC

We tested the performance of the OVC using two different LCP phase masks at wavelengths 633 nm and 1520 nm, respectively. The results of measurement contrast will be discussed in this section.

Figure 3 shows the layout of the OVC optical system, together with the phase mask, PSF on a different focal plane and a Lyot stop. Both the starlight and planet light are simulated by two point sources using two laser

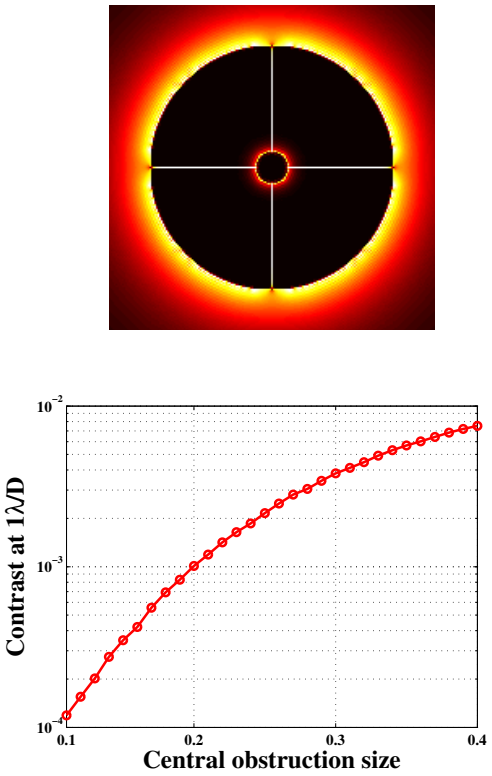

Fig. 5 The intensity distribution on Lyot stop plane (*top*). The contrast varies with the central obstruction size (*bottom*).

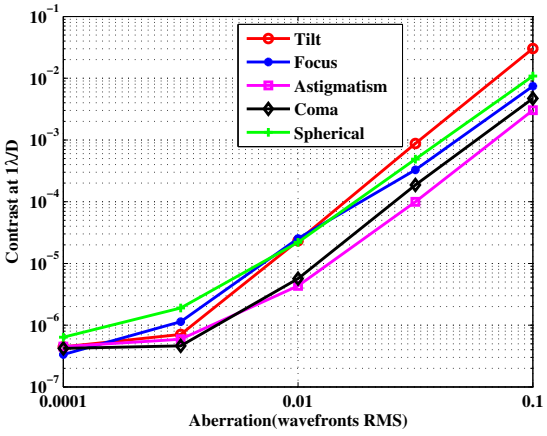

Fig. 6 The influence of low-order aberration on contrast.

light sources. A diaphragm is used as the entrance pupil and collimated light is focused on the phase mask. It is critical to exactly align the center of the PSF with the center of the phase mask. To achieve that, the LCP is installed on a three dimensional adjustable holder, which allows fine translations to locate its center perfectly on the focal point. A rotationally symmetric HWP generates the phase spiral in the vector vortex mask. Two LPCs optimized at 633 nm and 1520 nm respectively are manufactured by Thorlabs. The Thorlabs company tested the HWP when it was manufactured and the typical error associated with phase retardance distribution is on the order of ± 5 nm. The transmission of the LCPs is better than 97%. The Lyot stop is used to block light outside the pupil and is conjugated with the entrance pupil through our optical system. The diameters of the entrance pupil and the Lyot stop are 10 mm and 8 mm respectively. The detectors used in this test are 16-bit SBIG and 14-bit near infrared Xenics cameras.

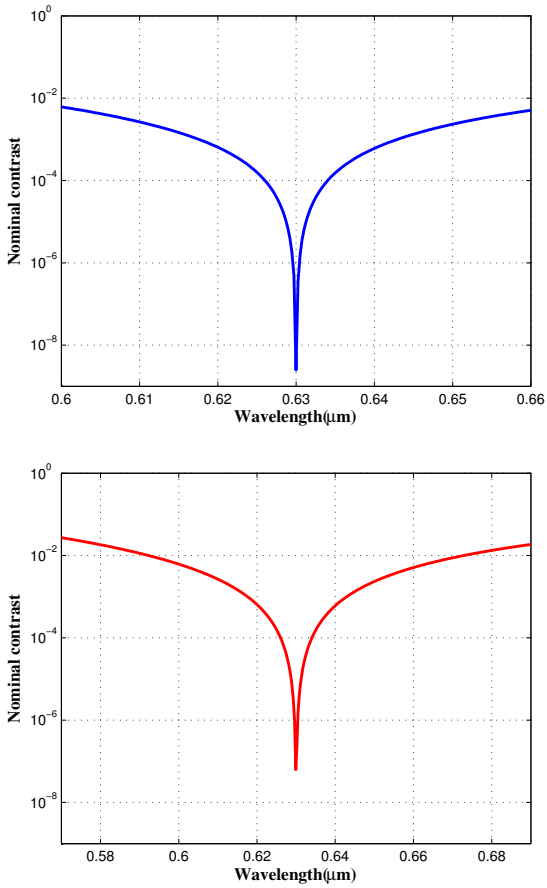

Fig. 7 Contrast provided by one layer LCP in 10% (*top*) and 20% (*bottom*) bandwidth.

To estimate the performance of OVC at 633 nm and 1520 nm, we first recorded 100∼1000 images with a specific exposure time in order to reduce the readout noise. To avoid saturation of non-coronagraphic images, we used neutral density filters and shorter exposures. The neutral density filters have been calibrated with the detector and could realize an attenuation factor of 10^{-3}. Then we removed the LCP phase mask to acquire non-coronagraphic images with the same exposure time. Also, all the images were subtracted with a median dark frame (derived from 100 individual dark frames). In

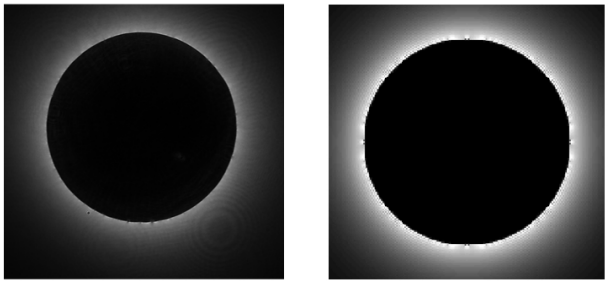

Fig. 8 Experimental pupil image at 633 nm after vortex phase mask (*left*) and theoretical pupil (*right*).

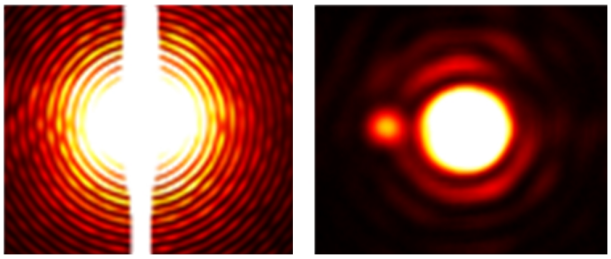

Fig. 9 Left: PSF without vortex phase mask. Simulated planet light is submerged in diffracted light from the star. Right: PSF with vortex phase mask. The planet is visible at a small angular distance.

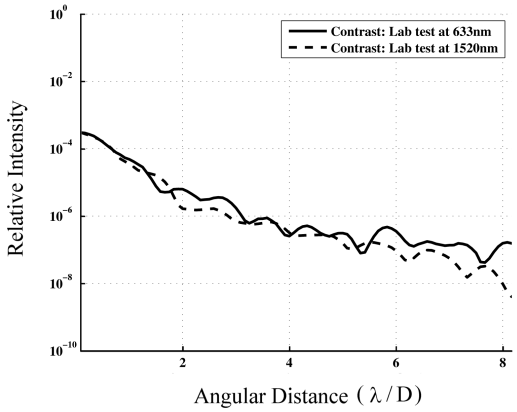

Fig. 10 Laboratory contrast test of our visible (*solid line*) and infrared (*dashed line*) optical vortex coronagraph.

this test, the peak to peak rejection metric, which means calculating the ratio of maximum intensity of the PSF without phase mask to the maximum intensity of the PSF with coronagraph, is adopted to quantify the OVC performance of attenuating starlight.

We first acquired an image of the coronagraphic exit pupil to verify that its performance is consistent with the theoretical simulation. Figure 8 shows the experimental and theoretical exit pupil images, in which input on-axis light is rejected inside the geometric pupil area. A Lyot stop is employed at the exit pupil plane to block the starlight. Figure 9 presents the PSF images without and with phase mask apodization in the final focal plane. The planet appears at an angular distance of $2\lambda/D$ with a contrast of 10^{-4} after vortex suppression. The attenuation ratio of the PSF peak with the OVC to the PSF peak without the OVC is about 3.03×10^{-4}.

Figure 10 shows that OVC can achieve a contrast of 10^{-6} at a small angular distance of $3\lambda/D$ in visible (633 nm). With the same method, we also tested the optical vortex coronagraph based on the infrared (1520 nm) LCP and almost the same result is shown in Figure 10 by the dashed line.

5 DISCUSSION

In conclusion, considering the high throughput, small IWA and complete 360° discovery area, the OVC is a promising technique for directly imaging exoplanets using small telescopes, which have more observation time available compared to large telescopes. In this paper, we describe our OVC based on an LCP, including numerical simulation and laboratory experiment demonstration. Both the visible and infrared vortex phase masks were used in the laboratory test. The simulation result shows that the OVC can achieve a contrast of 10^{-7} at $2\lambda/D$ with a reasonable number of sampled pixels. The laboratory test using visible and infrared LCPs manufactured by Thorlabs demonstrates that a deep suppression of the star peak (3300) can be achieved. Contrasts of 10^{-6} and $10^{-5.5}$ at angular distances $3\lambda/D$ and $2\lambda/D$ respectively have been realized in the visible and infrared wavelengths, respectively.

In the next step, this optical vortex coronagraph can be integrated with our ExAO to directly image young giant exoplanets with a contrast around $10^{-5.5}$ (Ren et al. 2012; Dou et al. 2015b) and ultimately be installed on 2∼4-m class telescopes for high contrast imaging. Also, our mature stepped-transmission filter based coronagraph can adopt this vortex phase mask to compose a hybrid coronagraph system and obtain better performance (Ren et al. 2010). Moreover, we are discussing and collaborating with Thorlabs to develop professional and high performance HWP with topological charge $l = 2, 4, 6$ according to our requirements. New progress will be presented in future publications.

Acknowledgements This work was supported by the National Natural Science Foundation of China (Grant Nos. 11661161011, 11433007, 11220101001, 11328302 and 11373005), the Strategic Priority Research Program of the Chinese Academy of Sciences (Grant No. XDA04075200), the International

Partnership Program of Chinese Academy of Sciences (Grant Nos. 114A32KYSB20160018 and 114A32KYSB20160057), as well as the special fund for astronomy of CAS (2015–2016). Part of the work described in this paper was carried out at California State University, Northridge, with support from the Mt. Cuba Astronomical Foundation.

References

Abe, L., Vakili, F., & Boccaletti, A. 2001, A&A, 374, 1161
Bottom, M., Shelton, J. C., Wallace, J. K., et al. 2016, PASP, 128, 075003
Delacroix, C., Absil, O., Forsberg, P., et al. 2013, A&A, 553, A98
Dou, J.-P., Ren, D.-Q., & Zhu, Y.-T. 2010, RAA (Research in Astronomy and Astrophysics), 10, 189
Dou, J., Ren, D., Zhao, G., et al. 2015a, ApJ, 802, 12
Dou, J., Ren, D., & Zhu, Y. 2015b, IAU General Assembly, 22, 2255996
Dou, J.-P., & Ren, D.-Q. 2016, ApJ, 832, 84
Foo, G., Palacios, D. M., & Swartzlander, Jr., G. A. 2005, Optics Letters, 30, 3308
Guyon, O. 2003, A&A, 404, 379
Guyon, O., Pluzhnik, E. A., Kuchner, M. J., Collins, B., & Ridgway, S. T. 2006, ApJS, 167, 81
Kasdin, N. J., Vanderbei, R. J., Spergel, D. N., & Littman, M. G. 2003, ApJ, 582, 1147
Kuchner, M. J., & Traub, W. A. 2002, ApJ, 570, 900
Liu, C.-C., Ren, D.-Q., Dou, J.-P., et al. 2015, RAA (Research in Astronomy and Astrophysics), 15, 453
Liu, C.-C., Ren, D.-Q., Zhu, Y.-T., Dou, J.-P., & Guo, J. 2016, RAA (Research in Astronomy and Astrophysics), 16, 73
Macintosh, B., Graham, J. R., Ingraham, P., et al. 2014, Proceedings of the National Academy of Science, 111, 12661
Mawet, D., Pueyo, L., Moody, D., Krist, J., & Serabyn, E. 2010, in Proc. SPIE, 7739, Modern Technologies in Space- and Ground-based Telescopes and Instrumentation, 773914
Mawet, D., Riaud, P., Absil, O., & Surdej, J. 2005, ApJ, 633, 1191
Mawet, D., Serabyn, E., Liewer, K., et al. 2009, Optics Express, 17, 1902
Mawet, D., Serabyn, E., Wallace, J. K., & Pueyo, L. 2011, Optics Letters, 36, 1506
McEldowney, S. C., Shemo, D. M., & Chipman, R. A. 2008b, Optics Express, 16, 7295
McEldowney, S. C., Shemo, D. M., Chipman, R. A., & Smith, P. K. 2008a, Optics Letters, 33, 134
Niv, A., Biener, G., Kleiner, V., & Hasman, E. 2006, Optics Express, 14, 4208
Ren, D., Dong, B., Zhu, Y., & Christian, D. J. 2012, PASP, 124, 247
Ren, D., Dou, J., & Zhu, Y. 2010, PASP, 122, 590
Ren, D., & Zhu, Y. 2007, PASP, 119, 1063
Rouan, D., Riaud, P., Boccaletti, A., Clénet, Y., & Labeyrie, A. 2000, PASP, 112, 1479
Rozas, D., Law, C. T., & Swartzlander, Jr., G. A. 1997, Journal of the Optical Society of America B Optical Physics, 14, 3054
Serabyn, E., Cady, E., Kern, B., & Mawet, D. 2014, in Aerospace Conference, IEEE, 1
Serabyn, E., Liewer, K., & Mawet, D. 2016, Optics Communications, 379, 64
Serabyn, E., Huby, E., Matthews, K., et al. 2017, AJ, 153, 43
Soummer, R., Aime, C., & Falloon, P. E. 2003, A&A, 397, 1161
Trauger, J. T., & Traub, W. A. 2007, Nature, 446, 771
Vasnetsov, M., & Staliunas, K. 1999, Optical vortices, 228 (Nova Science Pub Incorporated)
Vigan, A., Bonnefoy, M., Ginski, C., et al. 2016, A&A, 587, A55